A New Control Strategy for a Multi-Bus MV Microgrid Under Unbalanced Conditions

Mohsen Hamzeh, *Student Member, IEEE*, Houshang Karimi, *Member, IEEE*, and Hossein Mokhtari, *Member, IEEE*

***Abstract*—This paper proposes a new control strategy for the islanded operation of a multi-bus medium voltage (MV) microgrid. The microgrid consists of several dispatchable electronically-coupled distributed generation (DG) units. Each DG unit supplies a local load which can be unbalanced due to the inclusion of single-phase loads. The proposed control strategy of each DG comprises a proportional resonance (PR) controller with an adjustable resonance frequency, a droop control strategy, and a negative-sequence impedance controller (NSIC). The PR and droop controllers are, respectively, used to regulate the load voltage and share the average power components among the DG units. The NSIC is used to effectively compensate the negative-sequence currents of the unbalanced loads and to improve the performance of the overall microgrid system. Moreover, the NSIC minimizes the negative-sequence currents in the MV lines and thus, improving the power quality of the microgrid. The performance of the proposed control strategy is verified by using digital time-domain simulation studies in the PSCAD/EMTDC software environment.**

***Index Terms*—Distributed generation, medium voltage (MV) microgrid, negative-sequence current, power sharing, unbalance load, voltage control.**

I. Introduction

MEDIUM voltage (MV) microgrids will play a key role for active management and control of distribution network in the future smart grids. Moreover, the environmental issues and economical, social, and political interests make the role of MV microgrids even more important [1]. The recently presented concept of multi-microgrids is a motivation for proposing the concept of the higher voltage level structure of microgrids, e.g., MV level. A multi-microgrid consists of low voltage (LV) microgrids and distributed generation (DG) units connected to several adjacent MV feeders [2].

An MV microgrid may inherently be subjected to significant degrees of imbalance due to the presence of single-phase loads and/or DG units. Nevertheless, a microgrid should be able to operate under unbalanced conditions without any performance degradations. Based on the IEEE standards [3], [4], it is required that the voltage imbalance be maintained within 2% for sensitive equipments. In the presence of unbalanced loads, each DG unit must inject some part of the negative-sequence current to balance the load voltages.

Several methods have been proposed in the literature for the control and power management of microgrids [5]–[9]. An abc-frame control strategy is proposed in [10] which is robust to the unmodeled load dynamics. The proposed method employs the droop strategy for the power sharing.

The $G-H$ and $Q^{-}-G$ droop controls are employed to share harmonics and unbalanced currents among the DG units in an islanded microgrid [11], [12]. The proposed methods show good performance when the exact value of the line impedance is available. A combination of the deadbeat and repetitive control has been used to enhance the performance of a single-bus microgrid system in the presence of unbalanced and nonlinear loads [13]. However, the effectiveness of the proposed method is not investigated in the multi-bus microgrids. To overcome the impact of nonlinear and unbalanced loads, a proportional multi-resonant controller is proposed in [14]. The method employs the concept of generalization of virtual output impedance to deal with the nonlinear and harmonic loads. A droop-based control strategy for a microgrid has been proposed in [15]. The method improves the power quality and proper load sharing in both islanded and grid-connected modes in the presence of unbalanced and nonlinear loads. However, the paper assumes that the nonlocal loads are balanced.

This paper presents a new control strategy for an islanded microgrid consisting of several dispatchable electronically-interfaced three-wire DG units. The microgrid consists of several buses and operates in an MV level. Each DG unit supplies the local and nonlocal loads which can be unbalanced. The overall microgrid is controlled based on the decentralized control strategy, i.e., each DG unit is considered as a subsystem equipped with the proposed control strategy. However, it is assumed that each nonlocal bus (feeder) is equipped with a phase measurement unit (PMU) which transmits the phasor information of the feeder to the adjacent DG units.

The proposed control strategy of each DG comprises a voltage control loop, a droop controller and a negative-sequence output impedance controller. The voltage controller adaptively regulates the load voltage using a PR controller. The average power sharing between the DG units is carried out by the droop controller. However, the droop controller is not able to share the negative-sequence current resulting from the unbalanced loads. Thus, a new control strategy is proposed in this paper to efficiently share the negative-sequence current among the DG units. The proposed negative-sequence current controller adjusts the negative-sequence output impedance of its own DG such that the negative-sequence currents of the

Manuscript received November 01, 2011; revised November 06, 2011 and February 12, 2012; accepted April 01, 2012. Date of publication May 01, 2012; date of current version October 17, 2012. Paper no. TPWRS-01039-2011.

The authors are with the Center of Excellence in Power System Management & Control, Sharif University of Technology, Tehran, Iran (e-mail: m.hamzeh@ee.sharif.edu; houshang.karimi@sharif.edu; mokhtari@sharif.edu).

Color versions of one or more of the figures in this paper are available online at http://ieeexplore.ieee.org.

Digital Object Identifier 10.1109/TPWRS.2012.2193906

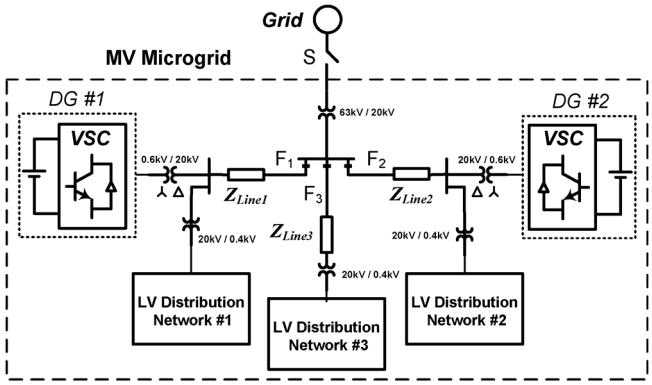

Fig. 1. MV multi-bus microgrid consisting of two DG units.

MV lines will be minimized. Thus, the power quality of the overall MV microgrid will be improved. The effectiveness of the proposed control strategy has been demonstrated through simulation studies conducted in the PSCAD/EMTDC environment. The simulation results show that the method is robust to load perturbations and effectively copes with the unbalanced conditions.

II. Multi-Bus MV Microgrid Structure

Fig. 1 shows a single-line diagram of a multi-bus MV microgrid which is composed of a 20-kV three-feeder distribution system and two electronically-coupled three-wire DG units. A combination of balanced and unbalanced loads are supplied through three radial feeders, F_1, F_2, and F_3. The DG units are connected to feeders F_1 and F_2 through step-up transformers and are assumed to be dispatchable. Thus, each DG unit can supply any amount of the real/reactive power within the pre-specified limits. Moreover, each DG must control its own power in a decentralized control manner. The loads are connected to the MV feeders via Y/Δ transformers, and therefore, the loads do not absorb any zero-sequence current from the MV feeders. Nevertheless, the load current can assume the negative-sequence component. In this paper, it is assumed that the microgrid system operates in the islanded mode. Therefore, the DG units are responsible for compensating the negative-sequence current of the unbalanced loads. The microgrid parameters are given in Table I.

III. Dynamic Model of a Three-wire DG Unit

Each DG unit including its series and capacitive (LC) filters can be considered as a subsystem of the microgird. To control the microgrid using the a decentralized control strategy, it is required that the dynamic model of each subsystem be derived first. Thus, in this section, the dynamic model of a three-wire DG unit, as a subsystem of the overall microgrid, is presented. Fig. 2 shows the circuit diagram of a three-wire DG subsystem.

The objective is to design a feedback control system to robustly regulate the load voltages in the presence of disturbances. It should be noted that since the microgrid system is a three-phase three-wire system, the zero-sequence of the currents become zero. Thus, using the Clarke transformation, the state space equation of the system in the stationary reference ($\alpha\beta$) frame is obtained as follows [16]:

TABLE I
Microgrid System Parameters

Parameter	Value	Comments
S_{base}	2.5 MVA	DG ratings
Z_{line1}	0.7 + j 1.57 Ω	5.7 km overhead line
Z_{line2}	0.5 + j 1.25 Ω	4 km overhead line
Z_{line3}	0.1 + j 0 Ω	2 km underground cable
L_{f1}, L_{f2}	0.3 mH	series filter inductance
R_{f1}, R_{f2}	0.0015 Ω	series filter resistance
C_{f1}, C_{f2}	2200 μF	filter capacitance
V_{dc}	1500 V	dc bus voltage
f_s	2 kHz	switching frequency
$P_{max_{DG_1}}, P_{max_{DG_2}}$	2.5 MW	
$Q_{max_{DG_1}}, Q_{max_{DG_2}}$	1.5 MVAr	
m_{DG_1}, m_{DG_2}	0.333 Hz/MW	P-f droop coefficients
n_{DG_1}, n_{DG_2}	0.0245 kV/MVAr	Q-V droop coefficients
$\bar{I}_{max_{DG_1}}$	0.3 kA	
$\bar{I}_{max_{DG_2}}$	0.5 kA	

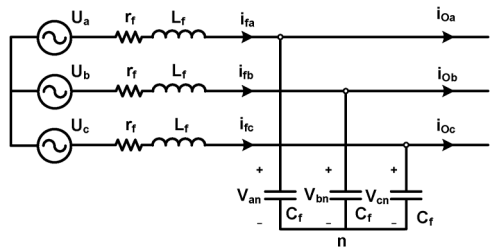

Fig. 2. Circuit diagram of a three-phase, three-wire DG unit.

$$\dot{\mathbf{X}} = \mathbf{AX} + \mathbf{BU} + \mathbf{EW}, \qquad \mathbf{Y} = \mathbf{CX} \tag{1}$$

where $\mathbf{X} = [v_\alpha, v_\beta, i_{f_\alpha}, i_{f_\beta}]^T$, $\mathbf{U} = [U_\alpha, U_\beta]^T$, $\mathbf{W} = [i_{o\alpha}, i_{o\beta}]^T$, $\mathbf{Y} = [v_\alpha, v_\beta]^T$ and

$$\mathbf{A} = \begin{bmatrix} 0 & 0 & \frac{1}{C_f} & 0 \\ 0 & 0 & 0 & \frac{1}{C_f} \\ -\frac{1}{L_f} & 0 & -\frac{r_f}{L_f} & 0 \\ 0 & -\frac{1}{L_f} & 0 & -\frac{r_f}{L_f} \end{bmatrix}, \quad \mathbf{B} = \begin{bmatrix} 0 & 0 \\ 0 & 0 \\ \frac{1}{L_f} & 0 \\ 0 & \frac{1}{L_f} \end{bmatrix}$$

$$\mathbf{E} = \begin{bmatrix} -\frac{1}{C_f} & 0 \\ 0 & -\frac{1}{C_f} \\ 0 & 0 \\ 0 & 0 \end{bmatrix}, \quad \mathbf{C} = \begin{bmatrix} 1 & 0 & 0 & 0 \\ 0 & 1 & 0 & 0 \end{bmatrix}. \tag{2}$$

The (1) in the Laplace domain is

$$V_{\alpha\beta}(s) = G_{(2\times2)}(s)U_{\alpha\beta}(s) - Z_{(2\times2)}(s)I_{o\alpha\beta}(s) \tag{3}$$

where $G_{(2\times2)}$ and $Z_{(2\times2)}(s)$ are

$$\begin{aligned} g_{12}(s) &= g_{21}(s) = z_{12}(s) = z_{21}(s) = 0 \\ g_{11}(s) &= g_{22}(s) = \frac{1}{L_f C_f s^2 + r_f C_f s + 1} \\ z_{11}(s) &= z_{22}(s) = \frac{L_f s + r_f}{L_f C_f s^2 + r_f C_f s + 1}. \end{aligned} \tag{4}$$

Equation (4) shows that the matrix transfer function of the DG subsystem is diagonal (completely decoupled) and can be viewed as two SISO control systems.

IV. Operation Principles of the Proposed Control Strategy

The proposed control strategy comprises 1) a voltage control, 2) a power sharing control loop, and 3) a negative-sequence current controller. The purpose of the voltage control loop is to keep the voltage of each bus of the microgrid within the acceptable limits. To eliminate the impact of the unknown dynamics (load dynamics), a feedforward controller is incorporated in the voltage control loop. In the $\alpha\beta$-frame, the reference signals are sinusoidal, and therefore, a PR controller is designed to ensure the excellent reference tracking [17], [18]. Moreover, since the frequency is determined by the droop control strategy and may deviate from its rated value, the proposed PR controller should adaptively adjust its parameters.

When the load is unbalanced, its power components will be oscillatory [19]. In this case, the conventional droop controller is used for sharing the average power components of the loads, and a negative-sequence output impedance control strategy is proposed to effectively share the oscillatory portions of the load power. It should be noted that each DG unit mainly compensates the oscillatory power of its local load. However, the oscillatory power components of the nonlocal loads are shared among all DG units. Therefore, the proposed control strategy improves the power quality of the overall microgrid. In the following sections, the control design procedure is explained in detail.

A. Proportional Resonance Controller With Non-Fixed Resonance Frequency

Since the matrix transfer function of the DG subsystem in the $\alpha\beta$-frame is diagonal, two identical SISO controllers can be independently designed for the quadrature axes α and β. Fig. 3 shows the block diagram of the voltage controller for α or β axis. The inner current control loop is a proportional controller which is used to increase the internal stability and to protect the voltage source converter (VSC) of the DG unit. The gain of the proportional controller is set such that the damping factor of the dominant poles of the inner loop system becomes 0.7. In this case, the gain is set to 2.9. The reference signal for the inner loop is generated by the PR controller as shown in Fig. 3.

The PR controller is designed using the SISO tools of MATLAB software. The designed controller provides good robust stability margins for the overall closed loop system, i.e., the phase and gain margins are 46° and 8 dB. The PR controller can be considered as a series connection of a fixed part $C(s)$ and a parameter dependent part $C_{AD}(s)$ as

$$C(s) = \frac{5756(s+40)(s^2+400\,\mathrm{s}+200,000)}{(s^2+4,000\,\mathrm{s}+8,000,000)},$$
$$C_{AD}(s) = \frac{1}{s^2+2\omega_{cut}s+\omega^2}. \quad (5)$$

Based on the internal model control (IMC) theory, zero steady state tracking error for a sinusoidal reference signal is achieved if the parameter ω equals the frequency of the reference signal V_{ref}. The frequency of the reference signal is determined by the droop controller and may slightly drift from its nominal value. Thus, the transfer function $C_{AD}(s)$ is implemented such that the parameter ω can adaptively be adjusted, as shown in Fig. 4.

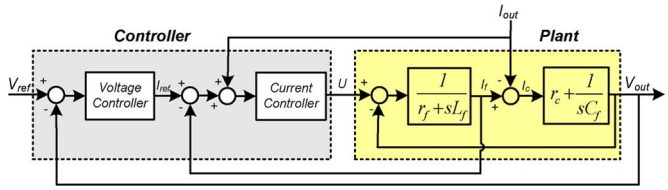

Fig. 3. Voltage controller structure in the $\boldsymbol{\alpha}$ or $\boldsymbol{\beta}$ axis.

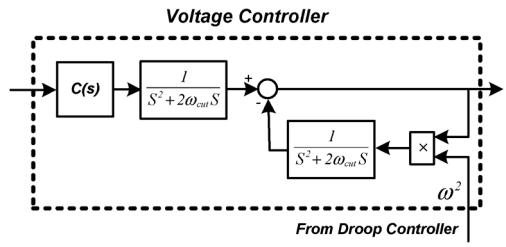

Fig. 4. Block diagram of the proposed PR controller.

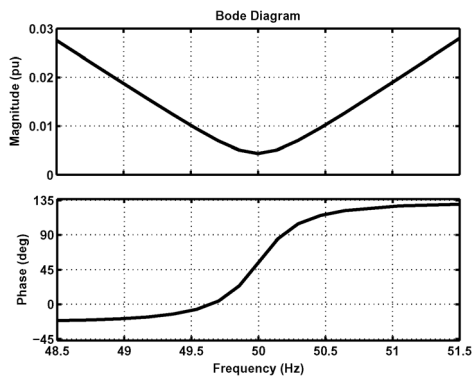

Fig. 5. Output impedance of the closed-loop DG system.

In this case, an excellent tracking is achieved even if the frequency of the reference signal deviates from its rated value. The damping factor $\omega_{cut} > 0$ is a very small number whose role will be explained in Section IV-D.

The output impedance of the DG is defined as

$$Z_{out}(s) = -\left.\frac{V_{out}(s)}{I_{out}(s)}\right|_{V_{ref}(s)=0} \quad (6)$$

where I_{out} and V_{out} are the terminal current and output voltage of the DG, respectively. Fig. 5 shows the frequency response of Z_{out} for the frequency interval [49 Hz, 51 Hz]. Note that the output impedance is computed for the closed-loop system according to Fig. 3 and (6). As shown in Fig. 5, the variation of Z_{out} is significant around 50 Hz. Thus, if the conventional PR controller with a fixed central frequency ω is used, the output impedance will be increased due to the frequency drift imposed by the droop controller. However, the proposed PR controller with an adjustable resonance frequency dynamically sets its central frequency to keep the output impedance at its minimum value.

B. Proposed Control System

Fig. 6 shows the block diagram of the proposed control system. The voltage controllers consist of two identical PR

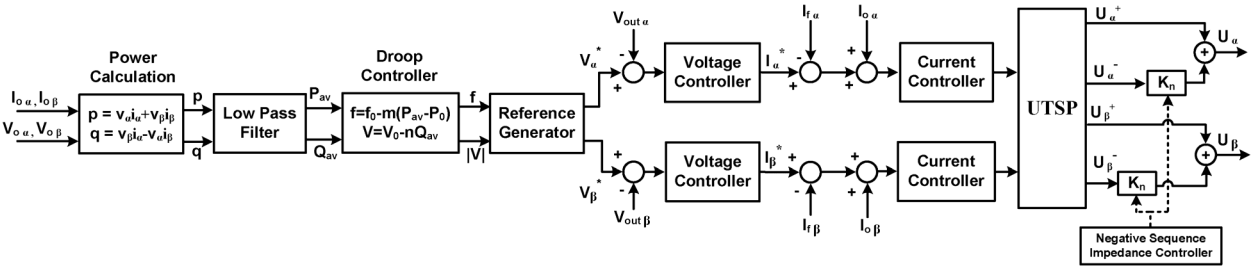

Fig. 6. Structure of the proposed control system.

controllers whose reference signals are determined by the droop control strategy. The droop characteristics, i.e., the droop coefficients m and n, are designed based on the DG rating power and the maximum allowable deviations for the frequency and voltage magnitude [20]. The instantaneous real and reactive powers are calculated based on the instantaneous real and reactive power theory proposed in [19]. A low pass filter with the cutoff frequency of 5 Hz is used to eliminate the double frequency ripples of the power components. The averaged power components are then applied to the droop controller to calculate frequency and voltage magnitude of the reference signals. The reference generator unit generates the reference signals for the PR controller. The outputs of the voltage controllers are considered as the reference signals for the current controllers. These signals are compared with the currents of the series filter and are added with the feedforward signals $i_{o\alpha}$ and $i_{o\beta}$. The resultant signals are then applied to the current controllers to generate the control signals U_α and U_β. To share the negative-sequence currents among the DG units, the signals U_α and U_β are decomposed into the symmetrical components using the unified three-phase signal processor (UTSP) proposed in [21].

The instantaneous negative-sequence components of the control signals are multiplied by a DC gain K_n which is generated by the NSIC. In this case, the negative-sequence output impedance of each DG is adjusted by manipulating the gain K_n. The positive- and negative-sequence components of the control signals are finally summed up to generate the control signals for the gating signal generator of the VSC.

C. Positive- and Negative-Sequence Models of Microgrid

To obtain the positive- and negative-sequence models of the overall microgrid, the dynamic model of each DG unit is obtained in the positive- and negative-sequence frames using Fig. 6. The positive-sequence voltages of the closed-loop system in the $\alpha\beta$-frame can be expressed as

$$V^+_{\alpha,\beta}(s) = H(s)V^*_{\alpha,\beta}(s) - Z^+_{out}(s)I^+_{o_{\alpha,\beta}}(s) \tag{7}$$

where $V^*_{\alpha,\beta}(s)$ is the voltage reference signal, and $I^+_{o_{\alpha,\beta}}(s)$ is the positive-sequence component of the DG current. $H(s)$ and $Z^+_{out}(s)$ denote the closed-loop transfer function from the reference signal to the output voltage of the DG and the positive-sequence output impedance, respectively.

The negative-sequence voltages of the closed-loop system is expressed as

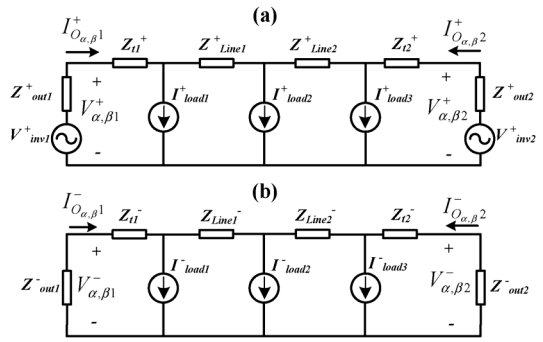

Fig. 7. (a) Positive- and (b) negative-sequence models of the two DG microgrid of Fig. 1.

$$V^-_{\alpha,\beta}(s) = -Z^-_{out}(s)I^-_{o_{\alpha,\beta}}(s) \tag{8}$$

where $Z^-_{out}(s)$ and $I^-_{o_{\alpha,\beta}}(s)$ are, respectively, the negative-sequence output impedance of the closed-loop system, and the DG negative-sequence current.

Based on (7) and (8), the positive- and negative-sequence models of the DG units of Fig. 1 are obtained, as shown in Fig. 7. The line and transformer parameters of both positive- and negative-sequence models are identical, and each load is modeled by a current source.

D. Negative-Sequence Current Sharing Strategy

To optimally share the negative-sequence currents between the DG units, the negative-sequence output impedance of each DG is adjusted by the parameter K_n [Figs. 6 and 7(b)]. The studies show that the negative-sequence output impedance is inversely proportional to K_n and increases as ω_{cut} is increased (Fig. 8). The magnitude of the negative-sequence output impedance at the system frequency, i.e., $|Z^-_{out}(j2\pi 50)|$, with respect to the parameter K_n for three values of ω_{cut} is shown in Fig. 8. The maximum value of the parameter K_n is determined such that the stability margins of the closed-loop system are not degraded. The maximum value for $Z^-_{out}(s)$, or equivalently, the minimum permissible value for K_n can be calculated based on the IEEE standards [3], [4], i.e.,

$$\frac{V^-_{\alpha,\beta}}{V^+_{\alpha,\beta}} < 0.02 \Rightarrow \frac{Z^-_{out}I^-_{o_{\alpha,\beta}}}{V^+_{\alpha,\beta}} < 0.02. \tag{9}$$

Moreover, the capability of a VSC in injecting the negative-sequence current is a limiting factor which, together with (9),

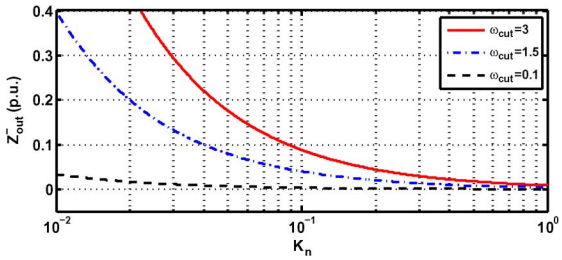

Fig. 8. Effect of K_n on the negative-sequence output impedance of the inverter.

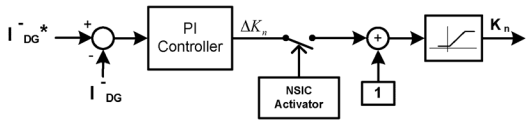

Fig. 9. NSIC structure.

determine the maximum value of the negative-sequence output impedance.

Fig. 9 shows the block diagram of the NSIC whose reference signal, I^{-*}_{DG}, is calculated as follows:

$$I^{-*}_{DG} = \sqrt{I^{-2}_{loc} + I^{-*2}_{nonloc} + 2I^{-}_{loc}I^{-*}_{nonloc}\cos\theta} \qquad (10)$$

where I^-_{loc} is the negative-sequence current of the local load, θ is the phase difference between I^-_{loc} and I^{-*}_{nonloc}, and I^{-*}_{nonloc} is

$$I^{-*}_{nonloc} = \frac{I^-_{max_{DGi}}}{\sum I^-_{max_{DGi}}} I^-_{nonloc}. \qquad (11)$$

In (11), $I^-_{max_{DG_i}}$ is the maximum negative-sequence current that the ith DG can inject, and I^-_{nonloc} is the amplitude of the negative-sequence current of the feeder supplying the nonlocal loads. It should be noted that if the impedances of the MV lines from the nonlocal loads to the adjacent feeders supplied by the DGs are known, the negative-sequence of output impedance can be adjusted by parameter K_n in an offline manner. However, to achieve optimal sharing of the negative-sequence current, it is required that the phasor of the negative-sequence current of each nonlocal load is measured and transmitted to all DG units. This can be performed by a low bandwidth communication link. In the context of the smart microgrids, the phase measurement units (PMUs) are used for this purpose. In the study system of Fig. 1, the PMUs are located at the 20-kV side of load transformers. One of the main advantages of the proposed method over the existing control strategies, i.e., [12]–[15], is that the phase-angle of the negative-sequence currents of the feeders are considered in the control loop. In some cases, therefore, the negative-sequence currents of the loads may cancel the effect of each other. In such cases, the DG units remain under balanced conditions.

It should be noted that the NSIC is not always in service. When the NSIC is disabled, the negative-sequence output impedance of the DG is kept at its minimum, Z^-_{min}, as indicated in Fig. 10. The flowchart of Fig. 10 determines when to activate the NSIC. According to this flowchart, the controller is enabled when 1) the capacity of a DG unit for injecting the negative-sequence current is reached, or 2) the local feeder with

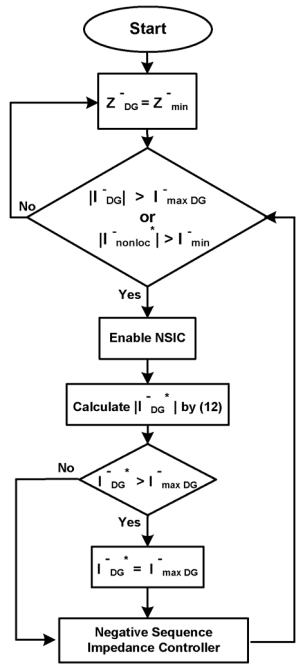

Fig. 10. Flowchart of negative-sequence current sharing strategy.

unbalanced load is not in an electrical proximity of a DG unit. Otherwise, the NSIC is disabled and the negative sequence of output impedance is kept constant at its minimum value.

When the proposed NSIC is enabled, a PI controller adjusts the parameter K_n to a desirable value. The PI controller is designed such that the NSIC closed-loop system has a low bandwidth. In this case, the coupling between the NSIC and other control loops will be minimized. Moreover, the NSIC is significantly slower than the droop and voltage controllers which prevents the undesirable transients in the microgrid.

V. Simulation Results

To verify the performance of the proposed control strategy, the MV microgrid of Fig. 1 has been simulated in PSCAD/EMTDC software. All DG units are equipped with the PR controller, droop control strategy, and the proposed NSIC. The loads are considered as a combination of a constant impedance and a constant power load. Feeder F_3 which is connected to a nonlocal load is supplied by the adjacent DGs. Two simulation case studies are carried out as detailed in the following sections.

A. Load Changes in Local Feeders

In this case study, while the microgrid system is initially operating under balanced conditions, a single-phase RL load with 240 kVA and $PF = 0.98$ is connected to the LV side of feeder F_1 at $t = 2$ s. Later at $t = 5$ s, an unbalanced three-phase RL load with 560 kVA and $PF = 0.9$ is connected to the same feeder. The real and reactive power of the three feeders for these changes are shown in Fig. 11. Since feeder F_1 becomes unbalanced, a double-frequency ripple is appeared in the instantaneous power components of this feeder. As it is observed, the double-frequency ripple is increased at $t = 5$ s due to the inclusion of the unbalanced three-phase load. Fig. 12 shows the positive- and negative-sequence components of the currents of all

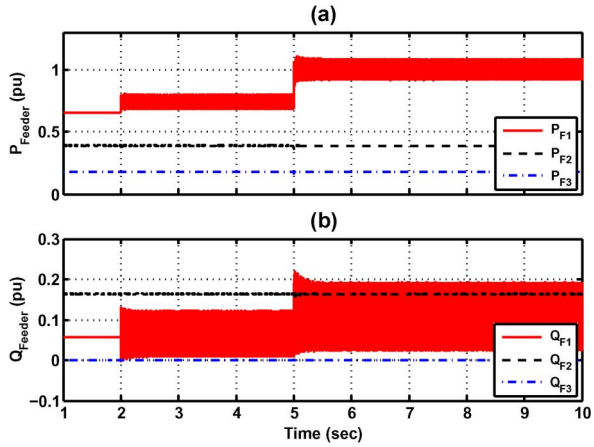

Fig. 11 Unbalanced load changes in feeder F_1 (a) instantaneous real, and (b) reactive power components.

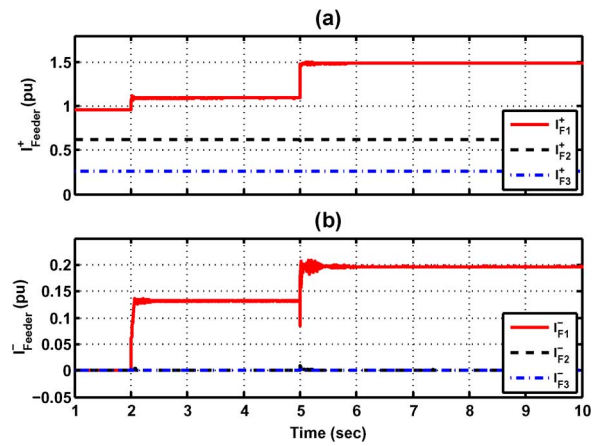

Fig. 12. Amplitude of (a) positive- and (b) negative-sequence currents of the feeders.

feeders. It is observed that the positive- and negative-sequence components step up at $t = 2$ s and $t = 5$ s.

Fig. 13 illustrates the instantaneous voltages of the DGs terminals prior and subsequent to the connection of the unbalanced load at $t = 5$ s. The voltage controller of each DG unit provides a set of regulated balanced voltages at its terminals. The microgrid system frequency is shown in Fig. 14. The variations of the frequency is imposed to the PR controller by the droop controller based on the $P - f$ characteristic.

Fig. 15 shows the negative-sequence output impedance and the negative-sequence current of the DG units. According to Fig. 10, the negative-sequence impedance of DG_1 is kept at its minimum level. Thus, the unbalanced conditions appeared at $t = 2$ s is locally compensated by the NSIC of DG_1. As depicted in Fig. 15(b), a small portion of the negative-sequence current is injected by DG_2. Fig. 16 shows the instantaneous real and reactive power components of the DG units during the load switchings. The double-frequency ripple component of each DG is proportional to its negative-sequence currents. The simulation studies show that if the PR controller does not maintain the output impedance of the positive-sequence of each DG at the minimum value, the average power of the DG shows low frequency oscillatory transients.

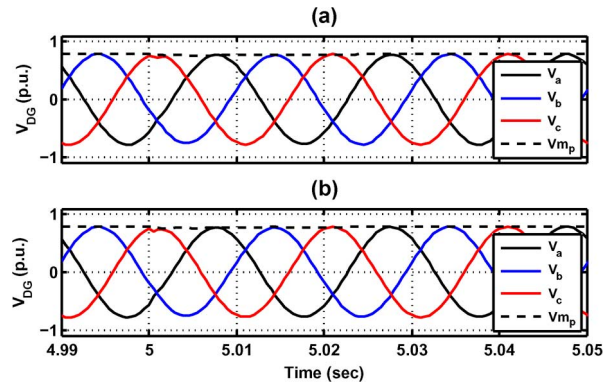

Fig. 13. Instantaneous voltages at DG terminals during unbalanced load changes in feeder F_1, (a) DG_1 and (b) DG_2.

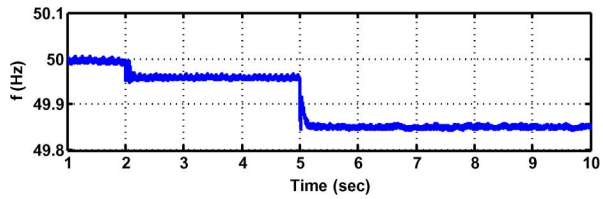

Fig. 14. Frequency of islanded microgrid during unbalanced load changes.

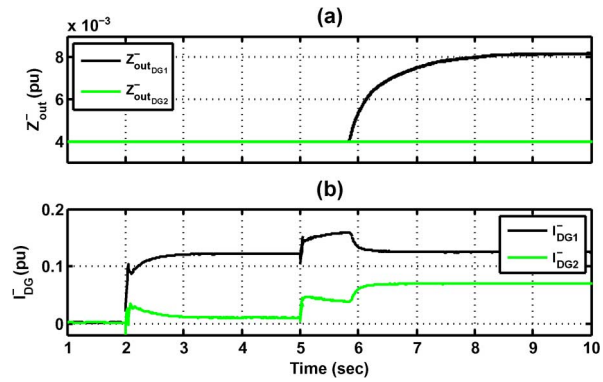

Fig. 15. (a) Negative-sequence output impedance of each DG, and (b) amplitude of negative-sequence current of DG units.

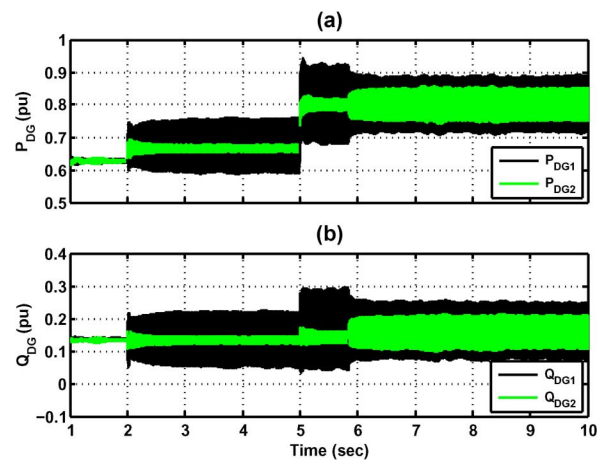

Fig. 16. Dynamic response of DG units to unbalanced load changes in feeder F_1: (a) real power, and (b) reactive power components of DG units.

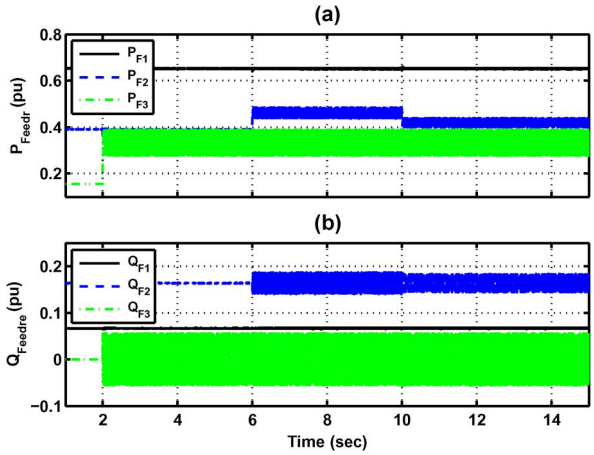

Fig. 17. Unbalanced load changes in feeders F_3 and F_2 (a, b) instantaneous real and reactive power of feeders.

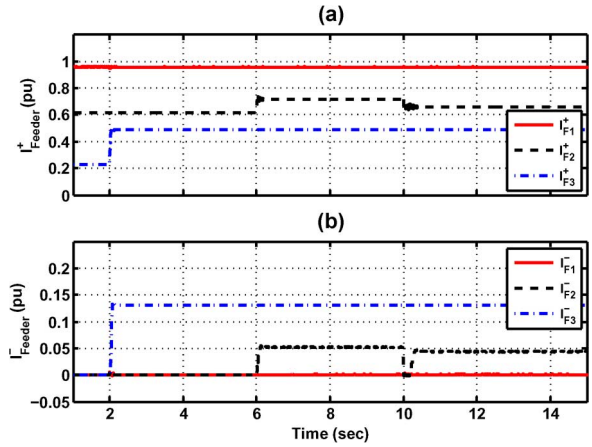

Fig. 18. Amplitude of (a) positive and (b) negative-sequence currents of the feeders.

When the second load switching occurs at $t = 5$ s, the negative-sequence current of feeder F_1 is increased until the capacity of the negative-sequence current injected by DG_1 is reached. In this case, according to Fig. 10, the NSIC of DG_1 is enabled and the controller starts to increase the negative-sequence impedance of DG_1 after about 0.85 s. The NSIC sets the reference signal of the negative-sequence current to $I^-_{max_{DG_1}}$. Therefore, the excess of the negative-sequence current of the local unbalanced loads is provided by DG_2.

B. Load Changes in Local and Nonlocal Feeders

In this case study, while the microgrid system is operating under the balanced conditions, the first load switching is applied at $t = 2$ s, where two 140-kW single-phase resistances are connected to the phases b and c at the LV side of feeder F_3. At $t = 6$ s, the second load switching is imposed to the LV side of feeder F_2, where two 100-kW single-phase resistive loads are connected to the phases b and c of the feeder. Finally, at $t = 10$ s, the single-phase resistance loads are disconnected from the phases b and c, and a 80-kW single-phase resistance is connected to phase a of feeder F_2. Figs. 17 and 18 show the instantaneous power components and the positive- and negative-sequence current components of the three feeders, respectively.

Subsequent to the load switching event at $t = 2$ s, the DG units activate their NSICs to share the demanded negative-sequence current by feeder F_3 after 0.9 s. In this case, the phasor $\vec{I}_{F_3}$ is measured by a PMU and transmitted to the adjacent DG units. The reference signal of the NSIC of each DG unit is calculated based on (10) and (11). As shown in Fig. 19(a), the controller of DG_1 increases its negative-sequence output impedance to adaptively share the negative-sequence current between the two DG units. As illustrated in Fig. 19(b), the negative-sequence current of each DG unit is proportionally compensated based on the values of $I^-_{max_{DG1}}$ and $I^-_{max_{DG2}}$.

Subsequent to the load change at $t = 6$ s, the reference signal of the negative-sequence current of DG_2 is changed to locally compensate the impact of its unbalanced load. However, the reference signal of the negative-sequence current of DG_1 is kept

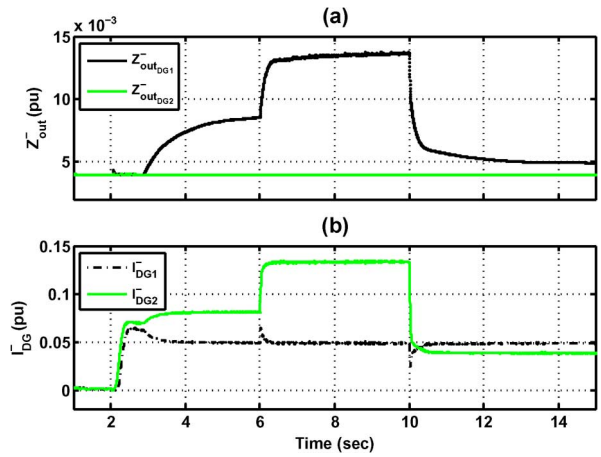

Fig. 19. (a) Negative-sequence output impedance, and (b) amplitude of negative-sequence current for each DG.

unchanged. In this case, $\cos\theta$ in (10) is positive and the amplitude of the reference signal for DG_2 is increased at $t = 6$ s. As shown in Fig. 19(b), the negative-sequence current of feeder F_2 is entirely provided by DG_2, and the negative-sequence current of feeder F_3 is compensated by both DG units. It should be noted that since the capacity of DG_2 in injecting the negative-sequence current is more than that of DG_1 (see Table I), its share is accordingly more.

When a load switching occurs at $t = 10$ s, $\cos\theta$ in (10) becomes negative, and the calculated reference signal for DG_2 becomes less than the negative-sequence current of its local load. In this case, the phase difference between the negative-sequence currents of the feeders are such that the unbalanced conditions cancel out the impact of each other in the overall microgrid, i.e., a portion of the negative-sequence current of feeder F_3 is compensated by the negative-sequence current of feeder F_2. Therefore, DG_2 reduces its negative sequence current as shown in Fig. 19(b).

VI. Conclusion

This paper presents a new control strategy for a multi-bus MV microgrid consisting of the dispatchable electronically-coupled

DG units and unbalanced loads. The negative-sequence current of a local load is completely compensated by its dedicated DG. However, the negative-sequence current of the nonlocal loads is shared among the adjacent DGs. The proposed control strategy is composed of a PR controller with non-fixed resonance frequency, a droop control, and a negative-sequence impedance controller (NSIC). The PR and droop controllers are, respectively, used to regulate the load voltage and to share the average power among the DG units. The NSIC is used to improve the performance of the microgrid system when the unbalanced loads are present. Moreover, the NSIC minimizes the negative-sequence currents in the MV lines, and thus, improving the power quality of the microgrid. The performance of the proposed control strategy is investigated by using digital time-domain simulation studies in the PSCAD/EMTDC software environment. The simulation results conclude that the proposed strategy:

- robustly regulates voltage and frequency of the microgrid;
- is able to share the average power among the DGs;
- effectively compensates the negative-sequence currents of local loads; and
- shares the negative-sequence current of the nonlocal loads such that the power quality of the overall microgrid is not degraded.

REFERENCES

[1] N. Hatziargyriou, H. Asano, R. Iravani, and C. Marnay, "Microgrids," *IEEE Power Energy Mag.*, vol. 5, pp. 78–94, Jul.–Aug. 2007.

[2] A. G. Madureira and J. A. P. Lopes, "Coordinated voltage support in distribution networks with distributed generation and microgrids," *IET Renew. Power Gener.*, vol. 3, pp. 439–454, Sep. 2009.

[3] *IEEE Recommended Practice for Monitoring Electric Power Quality*, IEEE Std. 1159, 2009.

[4] *IEEE Recommended Practice for Electric Power Distribution for Industrial Plants*, ANSI/IEEE Std. 141, 1993.

[5] R. Lasseter, "Microgrids," in *Proc. IEEE Power Eng. Soc. Winter Meeting*, 2002, pp. 305–308.

[6] M. H. J. Bollen and A. Sannino, "Voltage control with inverter-based distributed generation," *IEEE Trans. Power Del.*, vol. 20, no. 1, pp. 519–520, Jan. 2005.

[7] M. C. Chandrokar, D. M. Divan, and B. Banerjee, "Control of distributed ups systems," in *Proc. 25th Annu. IEEE PESC*, 1994, pp. 197–204.

[8] E. A. A. Coelho, P. C. Cortizo, and P. F. D. Garcia, "Small signal stability for parallel-connected inverters in stand-alone ac supply systems," *IEEE Trans. Ind. Appl.*, vol. 38, pp. 33–542, Mar./Apr. 2002.

[9] N. L. Soultanis, A. I. Tsouchnikas, N. D. Hatziargyriou, and J. Mahseredjian, "Dynamic analysis of inverter dominated unbalanced lv micro-grids," *IEEE Trans. Power Syst.*, vol. 22, no. 1, pp. 294–304, Feb. 2007.

[10] Y. Li, D. M. Vilathgamuwa, and P. C. Loh, "Design, analysis, and realtime testing of a controller for multibus microgrid system," *IEEE Trans. Power Electron.*, vol. 19, pp. 1195–1204, Sep. 2004.

[11] T. L. Lee and P. T. Cheng, "Design of a new cooperative harmonic filtering strategy for distributed generation interface converters in an islanding network," *IEEE Trans. Power Electron.*, vol. 22, pp. 1919–1927, Sep. 2007.

[12] P. Cheng, C. Chen, T. Lee, and S. Kuo, "A cooperative imbalance compensation method for distributed-generation interface converters," *IEEE Trans. Ind. Appl.*, vol. 45, pp. 805–815, Mar. 2009.

[13] M. B. Delghavi and A. Yazdani, "Islanded-mode control of electronically coupled distributed-resource units under unbalanced and nonlinear load conditions," *IEEE Trans. Power Del.*, vol. 26, no. 2, pp. 661–673, Apr. 2011.

[14] D. De and V. Ramanarayanan, "Decentralized parallel operation of inverters sharing unbalanced and non-linear loads," *IEEE Trans. Power Electron.*, vol. 25, pp. 3015–3025, Aug. 2010.

[15] R. Majumder, A. Ghosh, G. Ledwich, and F. Zare, "Load sharing and power quality enhanced operation of a distributed microgrid," *IET Renew. Power Gener.*, vol. 3, no. 2, pp. 109–119, 2009.

[16] M. N. Marwali and A. Keyhani, "Control of distributed generation systems-part i: Voltages and currents control," *IEEE Trans. Power Electron.*, vol. 19, pp. 1541–1550, Nov. 2004.

[17] A. Timbus, M. Liserre, R. Teodorescu, P. Rodriguez, and F. Blaabjerg, "Evaluation of current controllers for distributed power generation systems," *IEEE Trans. Power Electron.*, vol. 24, pp. 654–664, Mar. 2009.

[18] H. Karimi, A. Yazdani, and R. Iravani, "Robust control of an autonomous four-wire electronically-coupled distributed generation unit," *IEEE Trans. Power Del.*, vol. 26, no. 1, pp. 455–466, Jan. 2011.

[19] H. Akagi, E. H. Watanabe, and M. Aredes, *Instantaneous Power Theory and Applications to Power Conditioning*. New York: Wiley, 2007.

[20] M. C. Chandorkar, D. M. Divan, and R. Adapa, "Control of parallel connected inverters in standalone ac supply systems," *IEEE Trans. Ind. Appl.*, vol. 29, no. 1, pp. 136–143, Jan.–Feb. 1993.

[21] M. Karimi-Ghartemani and H. Karimi, "Processing of symmetrical components in time-domain," *IEEE Trans. Power Syst.*, vol. 22, no. 2, pp. 572–579, May 2007.

Mohsen Hamzeh (S'09) received the B.Sc. and M.Sc. degrees in electrical engineering from the University of Tehran, Tehran, Iran, in 2006 and 2008, respectively. He is currently pursuing the Ph.D. degree in electrical engineering at Sharif University of Technology, Tehran, Iran.

His research interests include distributed generation, microgrid control, and applications of power electronics in power distribution systems.

Houshang Karimi (S'03–M'07) received the B.Sc. and M.Sc. degrees from Isfahan University of Technology, Isfahan, Iran, in 1994 and 2000, respectively, and the Ph.D. degree from the University of Toronto, Toronto, ON, Canada, in 2007, all in electrical engineering.

He is currently an Assistant Professor in the Department of Electrical Engineering at Sharif University of Technology, Tehran, Iran. His research interests include control systems, distributed generations, and microgrid control.

Hossein Mokhtari (M'03) received the B.Sc. degree in electrical engineering from the University of Tehran, Tehran, Iran, in 1989, the M.Sc. degree in power electronics from the University of New Brunswick, Fredericton, NB, Canada, in 1994, and the Ph.D. degree in electrical engineering from the University of Toronto, Toronto, ON, Canada, in 1999.

Since 2000, he has been with the Department of Electrical Engineering, Sharif University of Technology, Tehran, where he is currently a Professor. His research interests include power quality, power electronics, and the application of power electronics in power systems.